

1 **Constraining uncertainties in particle wall-deposition correction during SOA**
2 **formation in chamber experiments**

3
4 T. Nah,¹ R. C. McVay,² J.R. Pierce,³ J. H. Seinfeld^{2,4} and N. L. Ng^{1,5*}

5
6 ¹*School of Chemical and Biomolecular Engineering, Georgia Institute of Technology, Atlanta, GA, USA*

7 ²*Division of Chemistry and Chemical Engineering, California Institute of Technology, Pasadena, CA, USA*

8 ³*Department of Atmospheric Science, Colorado State University, Fort Collins, CO, USA*

9 ⁴*Division of Engineering and Applied Science, California Institute of Technology, Pasadena, CA, USA*

10 ⁵*School of Earth and Atmospheric Sciences, Georgia Institute of Technology, Atlanta, GA, USA*

11
12 * To whom correspondence should be addressed: ng@chbe.gatech.edu
13

14 **Abstract**

15 The effect of vapor wall-deposition on secondary organic aerosol (SOA) formation has
16 gained significant attention; however, uncertainties in experimentally derived SOA mass
17 yields due to uncertainties in particle wall-deposition remain. Different approaches have
18 been used to correct for particle wall-deposition in SOA-formation studies, each having
19 its own set of assumptions in determining the particle wall-loss rate. In volatile and
20 intermediate-volatility organic compound systems in which SOA formation is governed
21 by kinetically limited growth, the effect of vapor wall-deposition on SOA mass yields can
22 be constrained by using high surface area concentrations of seed aerosol to promote the
23 condensation of SOA-forming vapors onto seed aerosol instead of the chamber walls.
24 However, under such high seed aerosol levels, the presence of significant coagulation
25 may complicate the particle wall-deposition correction. Here, we present a model
26 framework that accounts for coagulation in chamber studies in which high seed aerosol
27 surface area concentrations are used. For the α -pinene ozonolysis system, we find that,
28 after accounting for coagulation, SOA mass yields remain approximately constant when
29 large seed aerosol surface area concentrations ($\geq 8000 \mu\text{m}^2 \text{cm}^{-3}$) are used, consistent
30 with our prior study (Nah et al., 2016) that α -pinene ozonolysis SOA formation is
31 governed by quasi-equilibrium growth. In addition, we systematically assess the
32 uncertainties in the calculated SOA mass concentrations and yields between four
33 different particle wall-loss correction methods over the series of α -pinene ozonolysis
34 experiments. At low seed aerosol surface area concentrations ($< 3000 \mu\text{m}^2 \text{cm}^{-3}$), the
35 SOA mass yields at peak SOA growth obtained from the particle wall-loss correction

36 methods agree within 14 %. However, at high seed aerosol surface area concentrations (\geq
37 $8000 \mu\text{m}^2 \text{cm}^{-3}$), the SOA mass yields at peak SOA growth obtained from different
38 particle wall-loss correction methods can differ by as much as 58 %. These differences
39 arise from assumptions made in the particle wall-loss correction regarding the first-order
40 particle wall-loss rate. This study highlights the importance of accounting for particle
41 wall-deposition accurately during SOA-formation chamber experiments and assessing the
42 uncertainties associated with the application of the particle wall-deposition correction
43 method when comparing and using SOA mass yields measured in different studies.

44 **1. Introduction**

45 Secondary organic aerosol (SOA), which constitutes a large mass fraction of fine
46 atmospheric particulate matter, is formed from the oxidation of volatile and intermediate-
47 volatility organic compounds (VOCs and IVOCs) followed by gas-particle partitioning
48 (Kanakidou et al., 2005; Kroll and Seinfeld, 2008; Hallquist et al., 2009; Tsigaridis et al.,
49 2014). Laboratory chambers are typically used to study SOA formation from VOC and
50 IVOC oxidation in a controlled environment. SOA mass yields (Y), defined as the ratio
51 of mass concentration of SOA formed (ΔM_o) to the mass concentration of reacted
52 hydrocarbon (ΔHC) ($Y = \Delta M_o / \Delta\text{HC}$), are measured in these chamber experiments (Odum
53 et al., 1996; Odum et al., 1997a; Odum et al., 1997b). Interpretation of data derived from
54 such experiments is complicated by the fact that particles and SOA-forming vapors
55 deposit on the chamber walls throughout an experiment (Crump and Seinfeld, 1981;
56 McMurry and Grosjean, 1985; McMurry and Rader, 1985; Cocker et al., 2001; Weitkamp
57 et al., 2007; Pierce et al., 2008; Hildebrandt et al., 2009; Loza et al., 2010; Matsunaga and
58 Ziemann, 2010; Loza et al., 2012; Kokkola et al., 2014; McVay et al., 2014; Yeh and
59 Ziemann, 2014; Zhang et al., 2014; Yeh and Ziemann, 2015; Zhang et al., 2015;
60 Krechmer et al., 2016; La et al., 2016; McVay et al., 2016; Ye et al., 2016; Nah et al.,
61 2016). Failure to account for particle and vapor wall-losses accurately will result in
62 incorrect SOA mass yields, which will lead to flawed predictions of ambient SOA mass
63 concentrations (Cappa et al., 2016).

64 Particles deposit on the chamber walls via diffusion, gravitational settling and
65 electrostatic forces (Crump and Seinfeld, 1981; McMurry and Grosjean, 1985; McMurry

66 and Rader, 1985; Pierce et al., 2008). The rate at which particles deposit on chamber
67 walls depends on particle size. The particle wall-loss mechanism for uncharged particles
68 in an uncharged chamber is similar to that of the dry deposition of particles (Pierce et al.,
69 2008; Seinfeld and Pandis, 2016). Small particles are transported by Brownian diffusion
70 through the boundary layer adjacent to the chamber walls, while the loss of large particles
71 is governed by gravitational settling. Particle wall-loss rates are enhanced if the particles
72 and/or chamber walls are charged (McMurry and Grosjean, 1985; McMurry and Rader,
73 1985; Pierce et al., 2008). Smaller charged particles deposit more efficiently than larger
74 charged particles due to their larger Brownian diffusion rates and charge-to-mass ratios.

75 Several methods have been used to account for particle wall-deposition in SOA-
76 formation studies. In one particle wall-loss correction method, the rate of decay of
77 polydisperse inert seed aerosol (e.g., ammonium sulfate particles) is measured in periodic
78 seed-only experiments (Keywood et al., 2004; Pierce et al., 2008). Size-dependent
79 particle wall-deposition coefficients are then obtained by fitting a first-order exponential
80 decay to the measured particle number concentration decay in each size bin. The total
81 aerosol number concentration usually needs to be sufficiently low in these seed-only
82 experiments such that the effect of coagulation is negligible. In cases in which high seed
83 aerosol number concentrations are used, an aerosol dynamics model can be applied to
84 correct the particle wall-deposition coefficients for coagulation. Particle wall-loss in a
85 SOA formation experiment is then accounted for using these size-dependent particle
86 wall-deposition coefficients to obtain the total SOA mass concentration. A key
87 assumption of this approach is that the size-dependent particle wall-deposition
88 coefficients do not change between these seed-only and SOA-formation experiments.
89 Other previously reported particle wall-loss correction methods do not require the use of
90 separate seed-only experiments to characterize particle wall-loss rates. Instead, the
91 average loss rate of the total aerosol mass or number concentration is measured directly
92 during the SOA formation experiment (Carter et al., 2005; Pathak et al., 2007; Pierce et
93 al., 2008; Hildebrandt et al., 2009). The measured average particle loss rate is then
94 applied to the entire experiment to correct for particle wall-deposition. A key assumption
95 of this approach is that the particle wall-loss rate is not strongly dependent on particle
96 size, thus allowing for the overall particle wall-loss to be characterized by a single decay

97 rate coefficient. The extent to which these methods account for particle wall-deposition in
98 SOA-formation studies performed in a chamber, in which particle wall-loss rates are
99 known to strongly depend on particle size, is unclear. Therefore, SOA mass yield
100 uncertainties associated with the application of different particle wall-loss correction
101 methods need to be evaluated when comparing and using SOA mass yields measured in
102 different studies. This is the subject of the present work.

103 Previous studies have shown that SOA mass yields can be substantially
104 underestimated if the loss of SOA-forming vapors to chamber walls is not accounted for
105 (Matsunaga and Ziemann, 2010; McVay et al., 2014; Yeh and Ziemann, 2014; Zhang et
106 al., 2014; Yeh and Ziemann, 2015; Zhang et al., 2015; Krechmer et al., 2016; La et al.,
107 2016; McVay et al., 2016; Ye et al., 2016; Nah et al., 2016). Unlike particle wall-loss,
108 experimental methods for estimating vapor wall-loss rates in chambers are not yet well
109 established. However, the extent to which vapor wall-loss impacts SOA mass yields can
110 be characterized and quantified using time-dependent, parameterizable models that use
111 the measured SOA mass concentrations as model inputs (Zhang et al., 2014). Recent
112 studies have shown that the addition of large concentrations of seed aerosol can promote
113 gas-particle partitioning, and consequently increase SOA mass yields in VOC systems
114 where the condensation of SOA-forming vapors onto seed aerosol is kinetically limited
115 (i.e., the timescale for gas-particle equilibrium is competitive with or greater than those
116 for reaction and vapor wall-loss) (Riipinen et al., 2011; Zhang et al., 2012; McVay et al.,
117 2014; Zhang et al., 2014). In contrast, SOA growth is independent of seed aerosol surface
118 area in VOC systems in which the condensation of SOA-forming vapors onto seed
119 aerosol is governed by quasi-equilibrium growth (i.e., the timescale for gas-particle
120 equilibrium is less than those for reaction and vapor wall-loss) (Riipinen et al., 2011;
121 Zhang et al., 2012; McVay et al., 2014; McVay et al., 2016; Nah et al., 2016). Together,
122 these studies show that the role of gas-particle partitioning (i.e., kinetically limited vs.
123 quasi-equilibrium SOA growth) in influencing vapor wall-deposition can be inferred
124 from the relationship between SOA mass yields and seed aerosol surface area. However,
125 the use of high seed aerosol surface area concentrations in chamber studies may
126 complicate the particle wall-loss correction since (depending on the particle wall-loss
127 correction method used) the role of coagulation may need to be accounted for. It also

128 needs to be established how particle wall-deposition rates may change when different
129 seed aerosol concentrations (i.e., number, surface area and volume concentrations) and
130 size distributions are used. These uncertainties underscore the need to better constrain the
131 uncertainties associated with particle wall-loss correction since this correction will affect
132 the evaluation of the magnitude by which vapor wall-loss impacts chamber-derived SOA
133 mass yields.

134 In this work, we present results from targeted chamber experiments demonstrating
135 the change of size-dependent particle wall-deposition rates with different seed aerosol
136 concentrations (i.e., number, surface area and volume concentrations) and size
137 distributions. We also demonstrate how coagulation can be (and needs to be) accounted
138 for in experiments in which high seed aerosol surface area concentrations are used to
139 promote the condensation of SOA-forming vapors onto seed aerosol. Finally, we
140 compare SOA mass concentrations and yields in the canonical α -pinene ozonolysis
141 system obtained using four different particle wall-deposition correction methods, and
142 examine the uncertainties associated with each method. This work builds on our previous
143 study on the influence of seed aerosol surface area concentration and hydrocarbon
144 oxidation rate on vapor wall deposition and SOA mass yields in the α -pinene ozonolysis
145 system (Nah et al., 2016). In our previous study, we used a coupled vapor-particle
146 dynamics model to show that the condensation of SOA-forming vapors onto seed aerosol
147 in the α -pinene ozonolysis system is dominated by quasi-equilibrium growth. This
148 present work is aimed at understanding the uncertainties in the SOA mass yields due to
149 the application of different particle wall-deposition correction methods.

150 **2. Experimental**

151 Experiments were carried out in the Georgia Tech Environmental Chamber
152 (GTEC) facility (Boyd et al., 2015). A single FEP Teflon chamber (volume 13 m³) was
153 used for the entire study. Prior to each experiment, the chamber was flushed with dried,
154 purified air for > 24 h until the aerosol number concentration was < 30 cm⁻³. Experiments
155 were performed at < 5 % RH and 25 °C. NO_x mixing ratios in these experiments were < 1
156 ppb.

157 The dark α -pinene ozonolysis experimental procedure used in this study was
158 similar to that used in Nah et al. (2016). First, 22 ppm of cyclohexane (Sigma Aldrich, \geq
159 99.9 %), which served as an OH scavenger (\sim 440 times the initial α -pinene
160 concentration), was injected into the chamber. Based on the cyclohexane and α -pinene
161 concentrations in the chamber, the reaction rate of OH with cyclohexane is \sim 60 times
162 greater than that with α -pinene. Ammonium sulfate (AS) seed aerosol was next
163 introduced into the chamber via atomization of an aqueous AS solution. A known
164 concentration of α -pinene (Sigma Aldrich, > 99 %) (\sim 50 ppb in all experiments) was then
165 injected into the chamber. Finally, 500 ppb of ozone (O_3), which was generated by
166 passing purified air into a photochemical cell (Jelight 610), was introduced into the
167 chamber for 54.25 min after the seed aerosol and α -pinene concentrations in the chamber
168 had stabilized. The beginning of O_3 injection into the chamber marked the start of the
169 reaction (i.e., reaction time = 0 min). The O_3 mixing timescale was \sim 12 min for all
170 experiments. The O_3 injection time and mixing timescale were determined from separate
171 O_3 -only experiments (Nah et al., 2016). In seed-only experiments performed to measure
172 size-dependent particle wall-deposition coefficients, only AS seed aerosol was introduced
173 into the chamber. A gas chromatograph-flame ionization detector (GC-FID, Agilent
174 7890A) and O_3 monitor (Teledyne T400) measured the α -pinene and O_3 concentrations,
175 respectively. GC-FID measurements were taken 15 min apart. A high-resolution time-of-
176 flight aerosol mass spectrometer (HR-ToF-AMS, Aerodyne Research Inc.) measured the
177 aerosol elemental composition (DeCarlo et al., 2006; Canagaratna et al., 2015). A
178 scanning mobility particle sizer (SMPS, TSI), which consists of a differential mobility
179 analyzer (DMA, TSI 3081) and a condensation particle counter (CPC, TSI 3775),
180 measured the aerosol size distributions, number and volume concentrations.

181 The initial total AS seed aerosol surface area concentrations used in this study
182 were \sim 1000 and $\geq 8000 \mu\text{m}^2 \text{cm}^{-3}$ (referred to as “low-SA” and “high-SA” experiments,
183 respectively). To investigate how the seed aerosol size distribution may affect SOA mass
184 concentrations and yields, two different concentrations of AS solutions were used to
185 generate AS seed aerosol for both the seed-only and α -pinene ozonolysis experiments:
186 0.015 M or 0.05 M. In some experiments, both the 0.015 and 0.05 M AS solutions were
187 atomized into the chamber to achieve the desired total AS seed aerosol surface area

188 concentration. In these experiments, the 0.015 M AS solution was first atomized into the
189 chamber to achieve about half of the desired total AS seed aerosol surface area
190 concentration, followed by atomization of the 0.05 M AS solution. A summary of the
191 experimental conditions is shown in Table 1.

192 **3. Aerosol dynamics model**

193 An aerosol dynamics model is used to determine particle wall-deposition
194 coefficients that have been corrected for coagulation. This model was first described in
195 Pierce et al. (2008). In our work, we do not use the full Aerosol Parameter Estimation
196 (APE) model described in Pierce et al. (2008), but rather we employ the model used to
197 create the “No condensation” curve in Fig. 5 of the paper. This model includes only
198 coagulation and particle wall-loss, and it assumes that no condensation or evaporation
199 occurs during seed-only experiments, which are especially designed to measure particle
200 wall-deposition rates (experiments 1 through 6 in Table 1). Coagulation coefficients are
201 calculated from Table 13.1 in Seinfeld and Pandis (2016). The inputs to the model are the
202 raw time-dependent number distribution data measured by the SMPS during a particular
203 seed-only experiment. For each time step of the SMPS measurements, the model
204 calculates the decrease in the number concentration in each particle size bin due solely to
205 coagulation. The difference between this calculated decrease and the observed decrease
206 in the number concentration is attributed to particle wall-deposition, thus allowing size-
207 dependent particle wall-deposition coefficients to be determined. The model then re-
208 calculates the decrease in the number concentration for each particle size bin for that time
209 step due to both coagulation and particle wall-deposition using the deposition coefficients
210 just determined. The calculated decrease in the number concentration is again compared
211 to the measured values. This process of finding the size-dependent particle wall-
212 deposition rates is iterated using Newton’s method in order to converge upon particle
213 wall-deposition coefficients that fit the calculated number concentration decay to the
214 observed decay. The process is repeated for each SMPS measurement time step, yielding
215 size- and time-dependent particle wall-deposition coefficients. This process of finding the
216 size-dependent particle wall-deposition rates is carried out only when the number
217 concentration in the particle size bin of interest is > 20 particles cm^{-3} . For bins with ≤ 20

218 particles cm^{-3} , the deposition coefficient is not calculated during these time steps due to
219 uncertainties in the number counts in these bins leading to low confidence in the
220 determined particle wall-deposition rates. The deposition coefficients are averaged over
221 the entire experiment to yield coagulation-corrected size-dependent particle wall-
222 deposition coefficients.

223 **4. Results and discussion**

224 **4.1. Role of coagulation in particle wall-deposition corrections**

225 We performed a set of seed-only experiments using 0.015 M AS and/or 0.05 M
226 AS solutions to determine the extent to which size-dependent particle wall-loss rates
227 change with different seed aerosol concentrations and size distributions (experiments 1
228 through 6 in Table 1). The initial total AS seed aerosol surface area concentrations in the
229 low-SA-seed-only and high-SA-seed-only experiments are similar to those used in the α -
230 pinene ozonolysis experiments (i.e., ~ 1000 and $\geq 8000 \mu\text{m}^2 \text{cm}^{-3}$, respectively). Figure S1
231 shows the initial and final (420 min) number and volume size distributions for the seed-
232 only experiments. The initial number and volume size distributions in the low-SA-seed-
233 only experiments are smaller than those in the high-SA-seed-only experiments, regardless
234 of the concentration of the AS solution used to generate seed aerosol. As expected, all of
235 the size distributions shift to larger particle diameters as the experiment progresses due to
236 more efficient loss of smaller particles to the chamber walls and via coagulation as
237 compared to larger particles.

238 Figure 1 shows the size-dependent particle wall-deposition coefficients measured
239 directly in the low-SA-seed-only and high-SA-seed-only experiments (dashed lines). We
240 will refer to them as the *uncorrected* size-dependent particle wall-deposition coefficients
241 for the remainder of the discussion in this work since the effect of coagulation is assumed
242 to be negligible, and thus coagulation is not corrected for in these coefficients. The
243 uncorrected size-dependent particle wall-deposition coefficients are obtained directly
244 from SMPS measurements by fitting a first-order exponential decay to the measured
245 particle number concentration decay in each size bin. The uncorrected particle wall-
246 deposition coefficients are compared to those corrected for coagulation (shown as solid

247 lines in Fig. 1), which are obtained from the application of the aerosol dynamics model
248 (described in section 3) to the number distribution data measured by the SMPS. As
249 anticipated, a comparison of the uncorrected and coagulation-corrected size-dependent
250 particle wall-deposition coefficients indicates that coagulation has a smaller effect on the
251 deposition coefficients from the low-SA-seed-only experiments (experiments 1 through
252 4) compared to the high-SA-seed-only experiments (experiments 5 and 6). For example,
253 for particle diameters > 400 nm, the coagulation-corrected deposition coefficients for the
254 high-SA-seed-only experiments are up to an order of magnitude faster than the
255 uncorrected deposition coefficients. The smaller uncorrected deposition coefficients can
256 be attributed to particle formation (via coagulation) occurring simultaneously with
257 particle wall-deposition at these larger particle diameters in the high-SA-seed-only
258 experiments. A comparison of the change in total particle number concentration due to
259 coagulation alone (Fig. S2) shows that the low-SA-seed-only experiments (experiments 1
260 through 4) have smaller coagulation rates than the high-SA-seed-only experiments
261 (experiments 5 and 6). The observation that coagulation has a smaller effect on the
262 inferred deposition coefficients in the low-SA-seed-only experiments is expected since
263 these experiments involve significantly smaller particle number concentrations as
264 compared to the high-SA-seed-only experiments (2.5 to 4×10^4 particles cm^{-3} vs. 1 to 1.3
265 $\times 10^5$ particles cm^{-3}).

266 The coagulation-corrected size-dependent particle wall-deposition coefficients
267 obtained from the low-SA-seed-only experiments are generally in agreement. This is also
268 the case for the coagulation-corrected particle wall-deposition coefficients obtained from
269 the high-SA-seed-only experiments. Similar trends are observed for the uncorrected size-
270 dependent particle wall-deposition coefficients. Therefore, the concentration of the AS
271 solution(s) (i.e., 0.015 M and/or 0.05 M) used to generate the seed aerosol in seed-only
272 experiments does not influence the size-dependent particle wall-deposition coefficients.
273 The coagulation-corrected size-dependent particle wall-deposition coefficients obtained
274 from the low-SA-seed-only experiments are different from those obtained from the high-
275 SA-seed-only experiments. In addition, the minimum coagulation-corrected particle wall-
276 deposition coefficient for the low-SA-seed-only experiment (minimum particle diameter
277 ~ 300 nm) is lower than that of the high-SA-seed-only experiments (minimum particle

278 diameter ~530 nm). This result is surprising since the particle wall-deposition coefficients
279 are expected to depend solely on particle size once coagulation is accounted for.

280 We identify two possible explanations for the differences in the coagulation-
281 corrected particle wall-deposition coefficients. The first possibility is that there is a
282 difference in particle charging of the seed aerosol in the low-SA-seed-only and high-SA-
283 seed-only experiments. Particle wall-deposition is enhanced when charges are present on
284 particles (McMurry and Grosjean, 1985; McMurry and Rader, 1985; Pierce et al., 2008).
285 In all our experiments, a Boltzmann charge distribution was applied to the AS seed
286 aerosol by passing the particles through a Po-210 neutralizer prior to injection into the
287 chamber. However, it is possible that the particles are not fully neutralized before
288 entering the chamber, resulting in a difference in the true particle wall-deposition
289 coefficients due to the differences in particle charging between the experiments.

290 The second possible explanation for the differences in the coagulation-corrected
291 particle wall-deposition coefficients is that the Brownian coagulation kernel that we used
292 for our coagulation correction may not account for the entire coagulation rate in the
293 chamber. Coulombic and/or van der Waals forces may enhance the coagulation rates. We
294 performed a series of sensitivity tests to determine the extent to which the coagulation-
295 corrected size-dependent particle wall-deposition coefficients change as a function of
296 coagulation coefficients. In these tests, we scale the Brownian coagulation kernel by 1.1
297 and 1.5 uniformly across all particle sizes (as Coulombic and van der Waals
298 enhancements to coagulation have size dependence, these simple sensitivity tests do not
299 fully capture the changes due to either of these forces). Figure S3 shows results from
300 sensitivity tests performed on the seed-only experiments. These sensitivity tests show that
301 the coagulation-corrected particle wall-deposition coefficients in the low-SA-seed-only
302 and high-SA-seed-only experiments converge towards each other with increasing scale
303 factors on coagulation. However, with increasing coagulation scale factors, our derived
304 wall-deposition coefficients become negative at some particle sizes, which implies that
305 the size-independent coagulation scale factors are unrealistic. Future work should include
306 a more detailed investigation of the size-dependent coagulation enhancements provided
307 by Coulombic and van der Waals forces (which in turn requires knowledge about the

308 charge distribution and van der Waals forces), and it should include an investigation of
309 the charge-enhanced particle wall-losses (again requiring a knowledge of the charge
310 distribution). For the remainder of this work, we will use coagulation-corrected particle
311 wall-deposition coefficients with no enhancement to the coagulation rates (solid lines in
312 Figs. 1 and S3a).

313 We evaluated the effectiveness of the coagulation-corrected particle wall-
314 deposition coefficients (with no scaling of Brownian coagulation) in correcting for
315 particle wall-loss and coagulation by applying these coefficients to the SMPS data from
316 the seed-only experiments. The corrected volume concentration should level off at a
317 constant value (at the initial particle volume concentration) when particle wall-deposition
318 and coagulation are properly accounted for, since no condensation or evaporation occurs
319 during these experiments (due to the use of low-volatility AS seed aerosol and the
320 absence of condensable gases) and the wall-deposited particle volume concentration is
321 added back to the suspended particle volume concentration during particle wall-loss
322 correction. Figure S4 shows the raw and particle wall-deposition-corrected volume
323 concentrations. Coagulation-corrected size-dependent particle wall-deposition
324 coefficients are used for the particle wall-deposition correction shown in Fig. S4. Over all
325 experiments, the particle wall-deposition-corrected final volume concentration (i.e., at the
326 end of the experiment) is within 1 to 5 % of the initial volume concentration (Table S1).

327 **4.2. α -pinene ozonolysis**

328 We use the “size-dependent” method described in Loza et al. (2012) and Nah et
329 al. (2016) to correct for particle wall-deposition in the α -pinene ozonolysis experiments.
330 Briefly, size-dependent particle wall-deposition coefficients determined in separate seed-
331 only experiments (either through direct measurements or using an aerosol dynamics
332 model) are used to correct for particle wall-deposition in SOA-formation experiments.
333 Here we assume that particles cease to uptake SOA-forming vapors once they have
334 deposited, and hence the SOA mass present on deposited particles does not increase after
335 deposition. A key assumption of the “size-dependent” method is that the size-dependent
336 particle wall-deposition coefficients do not change significantly between experiments.
337 Seed-only experiments are performed regularly in the GTEC chamber. As shown in Fig.

338 1 (and Fig. 1 of Nah et al. (2016)), the uncorrected and coagulation-corrected size-
339 dependent particle wall-deposition coefficients are generally in line with each other at a
340 given seed aerosol surface area concentration. Since the seed-only and α -pinene
341 ozonolysis experiments were performed under similar experimental conditions (i.e., dark
342 conditions at $< 5\%$ RH and $25\text{ }^{\circ}\text{C}$), the size-dependent particle wall-deposition
343 coefficients are not expected to change significantly with reaction conditions for the
344 experiments presented in this study.

345 Since the focus of this work is the influence of coagulation and particle wall-
346 deposition on SOA mass yields, more high-SA α -pinene ozonolysis experiments
347 (experiments 9 through 12) were performed than low-SA experiments (experiments 7 and
348 8). To investigate the influence of coagulation on the SOA mass yields, both the
349 uncorrected and coagulation-corrected size-dependent particle wall-deposition
350 coefficients are used to correct for particle wall-deposition in the α -pinene ozonolysis
351 experiments. All the low-SA α -pinene ozonolysis data are particle wall-deposition-
352 corrected using uncorrected and coagulation-corrected size-dependent particle wall-
353 deposition coefficients from the low-SA-seed-only experiments, and all the high-SA α -
354 pinene ozonolysis data are corrected using uncorrected and coagulation-corrected particle
355 wall-deposition coefficients from the high-SA-seed-only experiments. Additional details
356 regarding the size-dependent particle wall-deposition coefficients used to correct for
357 particle wall-deposition in the different α -pinene ozonolysis experiments are provided in
358 Table 1. Figure S5 shows the raw and particle wall-deposition-corrected aerosol volume
359 concentrations for all the α -pinene ozonolysis experiments. In all the α -pinene ozonolysis
360 experiments, the volume concentrations that have been particle wall-deposition-corrected
361 using coagulation-corrected size-dependent particle wall-deposition coefficients (black)
362 reach peak values at reaction time ~ 100 min. In contrast, volume concentrations that have
363 been particle wall-deposition-corrected using uncorrected size-dependent particle wall-
364 deposition coefficients (blue) increase monotonically in the high-SA experiments
365 (experiments 9 through 12).

366 The SOA mass concentration is calculated from the product of the SOA density
367 with the difference of the particle wall-deposition-corrected volume concentration and the

368 initial seed aerosol volume concentration. We use an SOA density of 1.37 g cm^{-3} , which
369 was previously measured by Nah et al. (2016). Figure 2 shows the reaction profiles of the
370 low-SA α -pinene ozonolysis experiments. The SOA mass concentrations obtained using
371 the coagulation-corrected (Figs. 2a and 2b) and uncorrected (Figs. 2c and 2d) size-
372 dependent particle wall-deposition coefficients are sufficiently similar, which suggests
373 that coagulation plays a minor role in the low-SA experiments. As reported in Nah et al.
374 (2016), SOA growth typically occurs within 10 to 20 min of the start of the reaction. The
375 molar ratio of O_3 reacted to α -pinene reacted is approximately 1:1 (i.e., 50 ppb α -pinene
376 reacted with 50 ppb O_3), which indicates that O_3 reacts with α -pinene and not its
377 oxidation products. All the α -pinene reacts within 90 to 100 min of the start of reaction in
378 the 500 ppb O_3 experiments, and peak SOA levels occur at reaction time ~ 100 min. SOA
379 growth basically ceases once all the α -pinene has reacted, indicating that the first step of
380 α -pinene ozonolysis is rate-limiting and the first-generation products are condensable (
381 Gao et al., 2004a and 2004b; Ng et al., 2006; Chan et al., 2007). This result is expected
382 since α -pinene has a single double bond. The slight decrease in the SOA mass
383 concentrations after peak SOA growth may be due to imperfections in the particle wall-
384 deposition correction and/or vapor wall-deposition.

385 Figure 3 shows the reaction profiles of the high-SA α -pinene ozonolysis
386 experiments. In cases where the coagulation-corrected size-dependent particle wall-
387 deposition coefficients are used to correct for particle wall-deposition (Figs. 3a-d), the
388 SOA growth profile is similar to that of the low-SA experiments; SOA growth essentially
389 stops once all the α -pinene has reacted, as expected (Gao et al., 2004a and 2004b; Ng et
390 al. 2006; Chan et al., 2007). In contrast, when the uncorrected size-dependent particle
391 wall-deposition coefficients are used to correct for particle wall-deposition (Figs. 3e-h),
392 the SOA mass concentration continues to increase even after all the α -pinene has reacted.
393 This indicates that for the “size-dependent” method, SOA mass concentrations, and
394 consequently SOA mass yields, can be substantially overestimated when coagulation is
395 not accounted for during particle wall-deposition correction in high-SA experiments. This
396 underscores the importance of accounting for coagulation and particle wall-deposition
397 appropriately in chamber studies that employ high seed aerosol concentrations. We will
398 use SOA mass concentrations corrected using coagulation-corrected size-dependent

399 particle wall-deposition coefficients (solid lines in Fig. 1) for the remainder of the
400 discussion in this work.

401 Figure 4 shows the time-dependent SOA mass yields as a function of initial seed
402 aerosol surface area concentration for the α -pinene ozonolysis experiments. Also
403 included in Fig. 4 are results from Nah et al. (2016); SOA mass concentrations obtained
404 using coagulation-corrected size-dependent particle wall-deposition coefficients
405 determined in their study (Fig. S7 of Nah et al. (2016)). The SOA mass yield at peak
406 SOA growth remains approximately constant even at seed aerosol surface area
407 concentrations $\geq 8000 \mu\text{m}^2 \text{cm}^{-3}$. This confirms conclusions from our previous study that
408 the seed aerosol surface area concentration does not influence the partitioning of gas-
409 phase products to the particle phase in the α -pinene ozonolysis system (Nah et al., 2016).
410 As discussed in Nah et al. (2016), this behavior arises because SOA formation in the α -
411 pinene ozonolysis system is dominated by quasi-equilibrium growth (Saleh et al., 2013),
412 which occurs when the production rate of SOA-forming vapors is significantly slower
413 than that required to establish gas-particle equilibrium (Riipinen et al., 2011; Shiraiwa
414 and Seinfeld, 2012; Zhang et al., 2012). Gas-particle equilibrium is governed by the
415 amount of organic material in the system when the vapor and particle phases maintain
416 equilibrium. Thus, the seed aerosol surface area does not control the condensation rate of
417 SOA-forming vapors (McVay et al., 2014).

418 It is important to note that when the uncorrected size-dependent particle wall-
419 deposition coefficients (dashed lines in Fig. 1) are used for the particle wall-deposition
420 correction, the predicted SOA mass yield at peak SOA growth increases with seed
421 aerosol surface area (Fig. S6). This trend would lead to the incorrect conclusion that SOA
422 formation in the α -pinene ozonolysis system is governed by kinetically limited growth.
423 Therefore, this result further highlights the importance of accounting for coagulation and
424 particle wall-deposition properly in chamber studies (especially when high number
425 concentrations of seed aerosol are used) to avoid erroneous conclusions regarding the role
426 of gas-particle partitioning (quasi-equilibrium vs. kinetically limited SOA growth) in
427 affecting vapor wall-deposition and SOA mass yields in VOC systems.

428 **4.3. Uncertainties in SOA mass concentrations due to particle wall-loss corrections**

429 In the previous section, we showed that ignoring the role of coagulation in the
430 “size-dependent” particle wall-deposition correction method can contribute significant
431 errors to the calculated SOA mass concentrations and yields. These uncertainties could
432 lead to erroneous conclusions regarding the role of gas-particle partitioning in influencing
433 vapor wall-loss in the VOC system. Here, we investigate the uncertainties in the SOA
434 mass concentrations and yields as a result of the use of different particle wall-deposition
435 correction methods. We analyzed data from the α -pinene ozonolysis experiments using
436 four different commonly used particle wall-deposition correction methods. SOA mass
437 concentrations and yields obtained using the “size-dependent” particle wall-deposition
438 correction method (discussed in section 4.2) are compared to those obtained using the
439 “number averaged”, “volume averaged” and “inert tracer” methods, which are described
440 previously by Carter et al. (2005), Pathak et al. (2008) and Hildebrandt et al. (2009),
441 respectively. For the “size-dependent” method, only SOA mass concentrations and yields
442 corrected using coagulation-corrected size-dependent particle wall-deposition coefficients
443 (Fig. 4) will be used in the discussion presented here.

444 The “number averaged” and “volume averaged” methods use SMPS
445 measurements taken during SOA-formation studies. The “number averaged” method
446 involves measuring the average loss rate of the total aerosol number concentration after
447 peak SOA growth and then applying this first-order particle wall-deposition rate to the
448 entire experiment to correct for particle wall-loss (Carter et al., 2005). Since the average
449 loss rate of the total aerosol volume concentration is assumed to be the same as that of the
450 total aerosol number concentration, this first-order particle wall-deposition rate is also
451 applied to the total aerosol volume concentration data to determine the SOA mass
452 concentration. The “volume averaged” method involves measuring the average loss rate
453 of the total aerosol volume or mass concentration after peak SOA growth, and then
454 applying this first-order particle wall-deposition rate to the entire experiment to correct
455 for particle wall-loss (Pathak et al., 2007). Since the particle wall-deposition rate is
456 directly measured during SOA-formation experiments in the “number averaged” and
457 “volume averaged” methods, day-to-day variations of the particle wall-deposition rates
458 are accounted for. Unlike the “size-dependent” method, the “number averaged” and
459 “volume averaged” methods assume that particle wall-deposition rates depend weakly on

460 particle size, and hence particle wall-deposition can be represented by a single first-order
461 decay rate constant (Carter et al., 2005; Pathak et al., 2007; Pierce et al., 2008). It is
462 currently unclear if this assumption is valid for all seed aerosol concentrations (i.e.,
463 number, surface area and volume concentrations). The “inert tracer” method can be used
464 in SOA-formation studies where SMPS and AMS measurements are taken and non-
465 volatile sulfate seed aerosol is used (Hildebrandt et al., 2009). The SOA mass
466 concentration is calculated from the product of the initial seed aerosol sulfate mass
467 concentration (measured by the SMPS) to the time-dependent organic-to-sulfate
468 (Org/SO₄) ratio (measured by the HR-ToF-AMS). Examples of the application of the
469 “number averaged”, “volume averaged” and “inert tracer” methods to the α -pinene
470 ozonolysis data are shown in Fig. S7.

471 In original descriptions of the “size-dependent”, “number averaged” and “volume
472 averaged” methods, the authors assumed that particles cease to uptake SOA-forming
473 vapors once they have deposited to the walls, thus the SOA mass present on deposited
474 particles does not increase after deposition (Carter et al., 2005; Pathak et al., 2007; Loza
475 et al., 2012). In contrast, the “inert tracer” method assumes that deposited particles
476 continue to uptake suspended SOA-forming vapors at similar rates as suspended
477 particles, and hence the SOA mass present on the deposited particles will increase at the
478 same rate as those suspended (Hildebrandt et al., 2009). Therefore, SOA mass
479 concentrations and yields calculated by the “inert tracer” method are expected to be
480 higher than that calculated using the original descriptions of the “size-dependent”,
481 “number averaged” and “volume averaged” methods. It is important to note that the
482 assumption that deposited particles continue to uptake suspended SOA-forming vapors at
483 similar rates as suspended particles can also be applied to the “size-dependent”, “number
484 averaged” and “volume averaged” methods, which in turn will result in higher calculated
485 SOA mass concentrations and yields. However, we will use the “size-dependent”,
486 “number averaged” and “volume averaged” methods as originally described by Loza et
487 al. (2012), Carter et al. (2005) and Pathak et al. (2007), respectively, to correct for
488 particle wall-deposition in this discussion (i.e., deposited particles do not uptake SOA-
489 forming vapors). The “inert tracer” method will be used to evaluate its ability to predict
490 the role of gas-particle partitioning (quasi-equilibrium vs. kinetically limited SOA

491 growth) in affecting vapor wall-deposition and SOA mass yields in the α -pinene
492 ozonolysis system.

493 Figure 5 shows the SOA mass concentrations as a function of reaction time for the
494 four particle wall-deposition correction methods. For the low-SA experiments (Figs. 5a
495 and 5b), the SOA growth profiles obtained using the four different particle wall-
496 deposition correction methods are similar; SOA growth virtually stops after all the α -
497 pinene has reacted (at reaction time \sim 90 to 100 min). As expected, the SOA mass
498 concentrations calculated by the “inert tracer” method are higher than the SOA mass
499 concentrations calculated by the “size-dependent”, “number averaged” and “volume
500 averaged” methods. The SOA mass concentrations calculated by the “size-dependent”,
501 “number averaged” and “volume averaged” particle wall-deposition methods are
502 generally consistent with each other.

503 For the high-SA experiments (Figs. 5c to 5f), the SOA mass concentrations
504 calculated using the “size-dependent”, “volume averaged” and “inert tracer” methods
505 stop increasing after all the α -pinene has reacted (at reaction time \sim 90 to 100 min). In
506 contrast, the SOA mass concentrations calculated using the “number averaged” method
507 continued to increase even after all the α -pinene has reacted. These results suggest that
508 the calculated SOA mass concentrations and yields will be substantially overestimated if
509 the “number averaged” method is used to correct for particle wall-deposition in
510 experiments where high seed aerosol surface area concentrations are used. The erroneous
511 increase in the SOA mass concentration calculated by the “number averaged” method can
512 be attributed to the method’s assumption that the average loss rate of the total aerosol
513 volume concentration is the same as that of the total aerosol number concentration. The
514 “number averaged” method is effective in experiments where low concentrations of seed
515 aerosol are used since coagulation plays a minor role in affecting the average loss rate of
516 the total aerosol number concentration. However, it loses its accuracy in experiments
517 under high seed aerosol number concentrations because the average loss rate of the total
518 aerosol number concentration is driven by both coagulation and particle wall-deposition.
519 It is possible that the “number averaged” method may be an effective particle wall-
520 deposition correction method in these experiments if the measurements are corrected for

521 coagulation. The effect of coagulation on the SOA mass concentrations calculated by the
522 “volume averaged” and “inert tracer” methods is less prominent since coagulation does
523 not affect the aerosol volume and mass concentrations. Together, our results indicate that
524 the “size-dependent” (when coagulation is accounted for), “volume averaged” and “inert
525 tracer” methods are effective particle wall-deposition correction methods (regardless of
526 seed aerosol surface area concentrations) since the calculated SOA mass concentrations
527 stopped increasing after all the α -pinene has reacted.

528 Figure 6 shows the time-dependent SOA mass yields as a function of initial total
529 AS seed aerosol surface area concentration for the “number averaged”, “volume
530 averaged” and “inert tracer” particle wall-deposition correction methods. Also shown in
531 Fig. 6 are time-dependent SOA mass yields calculated using these three methods for the
532 α -pinene ozonolysis raw data reported by Nah et al. (2016). The time-dependent SOA
533 mass yields for the “number averaged”, “volume averaged” and “inert tracer” methods
534 (Fig. 6) are compared to those calculated using the “size-dependent” method (Fig. 4). For
535 seed aerosol surface area concentrations $< 3000 \mu\text{m}^2 \text{cm}^{-3}$, the SOA mass yields at peak
536 SOA growth (absolute values) calculated by the “size-dependent”, “number averaged”
537 and “volume averaged” methods agree within 14 % (Figs. 4, 6a and 6b). In contrast, for
538 seed aerosol surface area concentrations $\geq 8000 \mu\text{m}^2 \text{cm}^{-3}$, the SOA mass yields at peak
539 SOA growth calculated by the “number averaged” method range from 70.8 to 76.5 %
540 (Fig. 6a), while SOA mass yields at peak SOA growth calculated by the “size-dependent”
541 and “volume averaged” methods range from 17.2 to 27 % (Figs. 4 and 6b). As discussed
542 previously, this disagreement in the SOA mass yields is due to the treatment of (or lack
543 thereof) coagulation in the “number averaged” method. Failure to account for coagulation
544 in the “number averaged” method also resulted in the calculated SOA mass yields
545 increasing with seed aerosol surface area (Fig. 6a), which could lead to the incorrect
546 conclusion that SOA formation in the α -pinene ozonolysis system is governed by
547 kinetically limited growth. In contrast, the SOA mass yields calculated by the “volume
548 averaged” and “inert tracer” methods remain roughly constant despite the increase in AS
549 seed aerosol surface area (Figs. 6b and 6c), consistent with the results obtained using the
550 “size-dependent” method (Fig. 4).

551 **5. Conclusions**

552 An aerosol dynamics model can be used to account for coagulation in chamber
553 studies in which large seed aerosol surface area concentrations are used. Coagulation-
554 corrected size-dependent particle wall-deposition coefficients are obtained from the
555 application of the aerosol dynamics model to the experimental data from seed-only
556 experiments. Using these coagulation-corrected size-dependent particle wall-deposition
557 coefficients, we showed that the α -pinene ozonolysis SOA mass yields at peak SOA
558 growth remain approximately constant even when very high seed aerosol surface area
559 concentrations ($\geq 8000 \mu\text{m}^2 \text{cm}^{-3}$) are used. This confirms conclusions from our previous
560 study that the seed aerosol surface area concentration does not influence the partitioning
561 of α -pinene ozonolysis gas-phase products to the particle phase (Nah et al., 2016). Thus,
562 this indicates that SOA formation in the α -pinene ozonolysis system is dominated by
563 quasi-equilibrium growth, and that there are no significant limitations to vapor-particle
564 mass transfer (McVay et al., 2014; Nah et al., 2016).

565 The variability in the calculated SOA mass concentrations and yields between
566 four different particle wall-deposition correction methods is also evaluated for a series of
567 α -pinene ozonolysis experiments. In the experiments with low seed aerosol surface area
568 concentrations ($< 3000 \mu\text{m}^2 \text{cm}^{-3}$), the SOA mass yields obtained by the different particle
569 wall-deposition correction methods (i.e., the “size-dependent”, “number averaged” and
570 “volume averaged” methods) are generally consistent with one another. This indicates
571 that these three methods are effective in correcting for particle wall-deposition in
572 experiments that use low seed aerosol surface area concentrations. However, in the
573 experiments with high seed aerosol surface area concentrations ($\geq 8000 \mu\text{m}^2 \text{cm}^{-3}$), the
574 calculated SOA mass yields differ substantially. These differences arise from
575 assumptions made in the particle wall-deposition correction method regarding the
576 influence of coagulation on the first-order particle wall-loss rate. Specifically, we find
577 that coagulation needs to be accounted for in the “size-dependent” and “number
578 averaged” methods in order for them to be effective in chamber studies that use high seed
579 aerosol surface area concentrations. Coagulation does not need to be accounted for in the

580 “volume averaged” method since coagulation does not affect aerosol volume
581 concentrations.

582 Chamber experiments are subject to both particle and vapor wall-deposition.
583 While understanding the effect of vapor wall-deposition on the SOA mass yields is
584 critical, SOA mass yield uncertainties introduced by the particle wall-deposition
585 correction cannot be neglected. Results from this study underscore the importance of
586 constraining the SOA mass yield uncertainties introduced by the particle wall-deposition
587 correction regardless of the VOC system. Specifically, the effect of coagulation on
588 particle wall-deposition rates can be an important source of uncertainty not only in
589 determining SOA mass concentrations and yields, but also in evaluating the role of gas-
590 particle partitioning (quasi-equilibrium vs. kinetically limited SOA growth) in affecting
591 vapor wall-deposition in VOC systems. Here we showed that the condensation of SOA-
592 forming vapors in the α -pinene ozonolysis system can be erroneously concluded as
593 kinetically limited if coagulation is not accounted for in the “size-dependent” and
594 “number averaged” particle wall-deposition correction methods. Similar flawed
595 conclusions in other VOC systems may be drawn in chamber studies that use high seed
596 aerosol surface area concentrations to promote SOA formation but do not account for
597 coagulation. Therefore, we recommend accounting for coagulation when the “size-
598 dependent” and “number averaged” particle wall-deposition correction methods are used
599 in chamber studies that use high seed aerosol surface area concentrations (e.g., ≥ 3000
600 $\mu\text{m}^2 \text{cm}^{-3}$) to promote the condensation of SOA-forming vapors onto seed aerosol
601 regardless of VOC system. Alternatively, the “volume averaged” and “inert tracer”
602 methods can be used in chamber studies that use high seed aerosol surface area
603 concentrations. In addition, we suggest using multiple techniques (i.e., at least 2) to
604 correct for particle wall-loss in order to determine the effect of SOA mass yield
605 uncertainties introduced by particle wall-deposition correction. Complications arising
606 from particle and vapor wall deposition may also be potentially minimized by conducting
607 shorter duration chamber experiments. This can be achieved by using excess oxidant
608 concentrations, which increase the oxidation rate, and consequently reduce the time at
609 which peak SOA growth is achieved (Nah et al., 2016).

610 It is important to note that while results from the present study indicate that the
611 “volume averaged” and “inert tracer” methods are appropriate particle wall-deposition
612 correction methods for SOA-formation studies (regardless of seed aerosol surface area
613 concentrations) performed in the GTEC chamber in which the particle wall-loss rates
614 strongly depend on particle size, this may not be the case for all chambers. In addition to
615 particle size, particle wall-deposition rates depend on the chamber geometry, chamber
616 turbulence induced by mixing, and charge distribution on particles (Crump and Seinfeld,
617 1981; McMurry and Rader, 1985). All these factors need to be considered before one
618 decides which particle wall-deposition correction method to use in SOA-formation
619 studies. It is possible that the “volume averaged” and “inert tracer” methods may not be
620 appropriate particle wall-deposition correction methods for SOA-formation studies
621 performed in a chamber in which the particle wall-loss rates are even more strongly
622 dependent on particle size compared to the GTEC chamber. Therefore, we recommend
623 performing at least one separate seed-only experiment to measure the size-dependent
624 particle wall-deposition coefficients in order to probe the particle wall-deposition
625 characteristics of the chamber used before deciding on the particle wall-deposition
626 method to use in SOA-formation studies.

627 **Acknowledgements**

628 This research was funded by NSF grants 1455588 and AGS-1523500, and US
629 Environmental Protection Agency STAR grant (Early Career) RD-83540301. This
630 publication’s contents are solely the responsibility of the grantee and do not necessarily
631 represent the official views of the US EPA. Further, US EPA does not endorse the
632 purchase of any commercial products or services mentioned in the publication. R.C.
633 McVay was supported by a National Science Foundation Graduate Research Fellowship
634 under grant No. DGE-1144469.

635 **References**

636 Boyd, C. M., Sanchez, J., Xu, L., Eugene, A. J., Nah, T., Tuet, W. Y., Guzman, M. I., and
637 Ng, N. L.: Secondary organic aerosol formation from the β -pinene+NO₃ system: effect of

638 humidity and peroxy radical fate, *Atmos. Chem. Phys.*, 15, 7497-7522, 10.5194/acp-15-
639 7497-2015, 2015.

640 Canagaratna, M. R., Jimenez, J. L., Kroll, J. H., Chen, Q., Kessler, S. H., Massoli, P.,
641 Hildebrandt Ruiz, L., Fortner, E., Williams, L. R., Wilson, K. R., Surratt, J. D., Donahue,
642 N. M., Jayne, J. T., and Worsnop, D. R.: Elemental ratio measurements of organic
643 compounds using aerosol mass spectrometry: characterization, improved calibration, and
644 implications, *Atmos. Chem. Phys.*, 15, 253-272, 10.5194/acp-15-253-2015, 2015.

645 Cappa, C. D., Jathar, S. H., Kleeman, M. J., Docherty, K. S., Jimenez, J. L., Seinfeld, J.
646 H., and Wexler, A. S.: Simulating secondary organic aerosol in a regional air quality
647 model using the statistical oxidation model – Part 2: Assessing the influence of vapor
648 wall losses, *Atmos. Chem. Phys.*, 16, 3041-3059, 10.5194/acp-16-3041-2016, 2016.

649 Carter, W. P. L., Cocker, D. R., Fitz, D. R., Malkina, I. L., Bumiller, K., Sauer, C. G.,
650 Pisano, J. T., Bufalino, C., and Song, C.: A new environmental chamber for evaluation of
651 gas-phase chemical mechanisms and secondary aerosol formation, *Atmospheric*
652 *Environment*, 39, 7768-7788, 10.1016/j.atmosenv.2005.08.040, 2005.

653 Chan, A. W. H., Kroll, J. H., Ng, N. L., and Seinfeld, J. H.: Kinetic modeling of
654 secondary organic aerosol formation: effects of particle- and gas-phase reactions of
655 semivolatile products, *Atmospheric Chemistry and Physics*, 7, 4135-4147, 2007.

656 Cocker, D. R., Flagan, R. C., and Seinfeld, J. H.: State-of-the-art chamber facility for
657 studying atmospheric aerosol chemistry, *Environmental Science & Technology*, 35,
658 2594-2601, 10.1021/es0019169, 2001.

659 Crump, J. G., and Seinfeld, J. H.: Turbulent Deposition and Gravitational Sedimentation
660 of an Aerosol in a Vessel of Arbitrary Shape, *Journal of Aerosol Science*, 12, 405-415,
661 10.1016/0021-8502(81)90036-7, 1981.

662 DeCarlo, P. F., Kimmel, J. R., Trimborn, A., Northway, M. J., Jayne, J. T., Aiken, A. C.,
663 Gonin, M., Fuhrer, K., Horvath, T., Docherty, K. S., Worsnop, D. R., and Jimenez, J. L.:

664 Field-deployable, high-resolution, time-of-flight aerosol mass spectrometer, *Analytical*
665 *Chemistry*, 78, 8281-8289, 10.1021/ac061249n, 2006.

666 Gao, S., Ng, N. L., Keywood, M., Varutbangkul, V., Bahreini, R., Nenes, A., He, J. W.,
667 Yoo, K. Y., Beauchamp, J. L., Hodyss, R. P., Flagan, R. C., and Seinfeld, J. H.: Particle
668 phase acidity and oligomer formation in secondary organic aerosol, *Environmental*
669 *Science & Technology*, 38, 6582-6589, 10.1021/es049125k, 2004a.

670 Gao, S., Keywood, M., Ng, N. L., Surratt, J., Varutbangkul, V., Bahreini, R., Flagan, R.
671 C., and Seinfeld, J. H.: Low-molecular-weight and oligomeric components in secondary
672 organic aerosol from the ozonolysis of cycloalkenes and alpha-pinene, *J. Phys. Chem. A*,
673 108, 10147-10164, 10.1021/jp047466e, 2004b.

674 Hallquist, M., Wenger, J. C., Baltensperger, U., Rudich, Y., Simpson, D., Claeys, M.,
675 Dommen, J., Donahue, N. M., George, C., Goldstein, A. H., Hamilton, J. F., Herrmann,
676 H., Hoffmann, T., Iinuma, Y., Jang, M., Jenkin, M. E., Jimenez, J. L., Kiendler-Scharr,
677 A., Maenhaut, W., McFiggans, G., Mentel, T. F., Monod, A., Prevot, A. S. H., Seinfeld,
678 J. H., Surratt, J. D., Szmigielski, R., and Wildt, J.: The formation, properties and impact
679 of secondary organic aerosol: current and emerging issues, *Atmospheric Chemistry and*
680 *Physics*, 9, 5155-5236, 2009.

681 Hildebrandt, L., Donahue, N. M., and Pandis, S. N.: High formation of secondary organic
682 aerosol from the photo-oxidation of toluene, *Atmospheric Chemistry and Physics*, 9,
683 2973-2986, 2009.

684 Kanakidou, M., Seinfeld, J. H., Pandis, S. N., Barnes, I., Dentener, F. J., Facchini, M. C.,
685 Van Dingenen, R., Ervens, B., Nenes, A., Nielsen, C. J., Swietlicki, E., Putaud, J. P.,
686 Balkanski, Y., Fuzzi, S., Horth, J., Moortgat, G. K., Winterhalter, R., Myhre, C. E. L.,
687 Tsigaridis, K., Vignati, E., Stephanou, E. G., and Wilson, J.: Organic aerosol and global
688 climate modelling: a review, *Atmospheric Chemistry and Physics*, 5, 1053-1123, 2005.

689 Keywood, M. D., Varutbangkul, V., Bahreini, R., Flagan, R. C., and Seinfeld, J. H.:
690 Secondary organic aerosol formation from the ozonolysis of cycloalkenes and related

691 compounds, *Environmental Science & Technology*, 38, 4157-4164, 10.1021/es035363o,
692 2004.

693 Kokkola, H., Yli-Pirila, P., Vesterinen, M., Korhonen, H., Keskinen, H., Romakkaniemi,
694 S., Hao, L., Kortelainen, A., Joutsensaari, J., Worsnop, D. R., Virtanen, A., and Lehtinen,
695 K. E. J.: The role of low volatile organics on secondary organic aerosol formation,
696 *Atmospheric Chemistry and Physics*, 14, 1689-1700, 10.5194/acp-14-1689-2014, 2014.

697 Krechmer, J. E., Pagonis, D., Ziemann, P. J., and Jimenez, J. L.: Quantification of Gas-
698 Wall Partitioning in Teflon Environmental Chambers Using Rapid Bursts of Low-
699 Volatility Oxidized Species Generated in Situ, *Environmental Science & Technology*, 50,
700 5757-5765, 10.1021/acs.est.6b00606, 2016.

701 Kroll, J. H., and Seinfeld, J. H.: Chemistry of secondary organic aerosol: Formation and
702 evolution of low-volatility organics in the atmosphere, *Atmospheric Environment*, 42,
703 3593-3624, 10.1016/j.atmosenv.2008.01.003, 2008.

704 La, Y. S., Camredon, M., Ziemann, P. J., Valorso, R., Matsunaga, A., Lannuque, V., Lee-
705 Taylor, J., Hodzic, A., Madronich, S., and Aumont, B.: Impact of chamber wall loss of
706 gaseous organic compounds on secondary organic aerosol formation: explicit modeling
707 of SOA formation from alkane and alkene oxidation, *Atmos. Chem. Phys.*, 16, 1417-
708 1431, 10.5194/acp-16-1417-2016, 2016.

709 Loza, C. L., Chan, A. W. H., Galloway, M. M., Keutsch, F. N., Flagan, R. C., and
710 Seinfeld, J. H.: Characterization of Vapor Wall Loss in Laboratory Chambers,
711 *Environmental Science & Technology*, 44, 5074-5078, 10.1021/es100727v, 2010.

712 Loza, C. L., Chhabra, P. S., Yee, L. D., Craven, J. S., Flagan, R. C., and Seinfeld, J. H.:
713 Chemical aging of m-xylene secondary organic aerosol: laboratory chamber study,
714 *Atmospheric Chemistry and Physics*, 12, 151-167, 10.5194/acp-12-151-2012, 2012.

715 Matsunaga, A., and Ziemann, P. J.: Gas-Wall Partitioning of Organic Compounds in a
716 Teflon Film Chamber and Potential Effects on Reaction Product and Aerosol Yield

717 Measurements, *Aerosol Science and Technology*, 44, 881-892,
718 10.1080/02786826.2010.501044, 2010.

719 McMurry, P. H., and Grosjean, D.: Gas and Aerosol Wall Losses in Teflon Film Smog
720 Chambers, *Environmental Science & Technology*, 19, 1176-1182, 10.1021/es00142a006,
721 1985.

722 McMurry, P. H., and Rader, D. J.: Aerosol Wall Losses in Electrically Charged
723 Chambers, *Aerosol Science and Technology*, 4, 249-268, 10.1080/02786828508959054,
724 1985.

725 McVay, R. C., Cappa, C. D., and Seinfeld, J. H.: Vapor-Wall Deposition in Chambers:
726 Theoretical Considerations, *Environmental Science & Technology*, 48, 10251-10258,
727 10.1021/es502170j, 2014.

728 McVay, R. C., Zhang, X., Aumont, B., Valorso, R., Camredon, M., La, Y. S., Wennberg,
729 P. O., and Seinfeld, J. H.: SOA formation from the photooxidation of α -pinene:
730 systematic exploration of the simulation of chamber data, *Atmos. Chem. Phys.*, 16, 2785-
731 2802, 10.5194/acp-16-2785-2016, 2016.

732 Nah, T., McVay, R. C., Zhang, X., Boyd, C. M., Seinfeld, J. H., and Ng, N. L.: Influence
733 of seed aerosol surface area and oxidation rate on vapor wall deposition and SOA mass
734 yields: a case study with α -pinene ozonolysis, *Atmos. Chem. Phys.*, 16, 9361-9379,
735 10.5194/acp-16-9361-2016, 2016.

736 Ng, N. L., Kroll, J. H., Keywood, M. D., Bahreini, R., Varutbangkul, V., Flagan, R. C.,
737 Seinfeld, J. H., Lee, A., and Goldstein, A. H.: Contribution of first- versus second-
738 generation products to secondary organic aerosols formed in the oxidation of biogenic
739 hydrocarbons, *Environmental Science & Technology*, 40, 2283-2297,
740 10.1021/es052269u, 2006.

741 Odum, J. R., Hoffmann, T., Bowman, F., Collins, D., Flagan, R. C., and Seinfeld, J. H.:
742 Gas/Particle Partitioning and Secondary Organic Aerosol Yields, *Environmental Science
743 & Technology*, 30, 2580-2585, 10.1021/es950943+, 1996.

744 Odum, J. R., Jungkamp, T. P. W., Griffin, R. J., Flagan, R. C., and Seinfeld, J. H.: The
745 atmospheric aerosol-forming potential of whole gasoline vapor, *Science*, 276, 96-99,
746 10.1126/science.276.5309.96, 1997a.

747 Odum, J. R., Jungkamp, T. P. W., Griffin, R. J., Forstner, H. J. L., Flagan, R. C., and
748 Seinfeld, J. H.: Aromatics, reformulated gasoline, and atmospheric organic aerosol
749 formation, *Environmental Science & Technology*, 31, 1890-1897, 10.1021/es9605351,
750 1997b.

751 Pathak, R. K., Stanier, C. O., Donahue, N. M., and Pandis, S. N.: Ozonolysis of alpha-
752 pinene at atmospherically relevant concentrations: Temperature dependence of aerosol
753 mass fractions (yields), *J. Geophys. Res.-Atmos.*, 112, 8, 10.1029/2006jd007436, 2007.

754 Pierce, J. R., Engelhart, G. J., Hildebrandt, L., Weitkamp, E. A., Pathak, R. K., Donahue,
755 N. M., Robinson, A. L., Adams, P. J., and Pandis, S. N.: Constraining particle evolution
756 from wall losses, coagulation, and condensation-evaporation in smog-chamber
757 experiments: Optimal estimation based on size distribution measurements, *Aerosol
758 Science and Technology*, 42, 1001-1015, 10.1080/02786820802389251, 2008.

759 Riipinen, I., Pierce, J. R., Yli-Juuti, T., Nieminen, T., Häkkinen, S., Ehn, M., Junninen,
760 H., Lehtipalo, K., Petäjä, T., Slowik, J., Chang, R., Shantz, N. C., Abbatt, J., Leaitch, W.
761 R., Kerminen, V. M., Worsnop, D. R., Pandis, S. N., Donahue, N. M., and Kulmala, M.:
762 Organic condensation: a vital link connecting aerosol formation to cloud condensation
763 nuclei (CCN) concentrations, *Atmos. Chem. Phys.*, 11, 3865-3878, 10.5194/acp-11-3865-
764 2011, 2011.

765 Saleh, R., Donahue, N. M., and Robinson, A. L.: Time Scales for Gas-Particle
766 Partitioning Equilibration of Secondary Organic Aerosol Formed from Alpha-Pinene
767 Ozonolysis, *Environmental Science & Technology*, 47, 5588-5594, 10.1021/es400078d,
768 2013.

769 Seinfeld, J. H., and Pandis, S. N.: *Atmospheric chemistry and physics : from air pollution
770 to climate change*, Third edition. ed., John Wiley & Sons, Inc., Hoboken, New Jersey,
771 xxvi, 1120 pages pp., 2016.

772 Shiraiwa, M., and Seinfeld, J. H.: Equilibration timescale of atmospheric secondary
773 organic aerosol partitioning, *Geophys. Res. Lett.*, 39, 6, 10.1029/2012gl054008, 2012.

774 Tsigaridis, K., Daskalakis, N., Kanakidou, M., Adams, P. J., Artaxo, P., Bahadur, R.,
775 Balkanski, Y., Bauer, S. E., Bellouin, N., Benedetti, A., Bergman, T., Berntsen, T. K.,
776 Beukes, J. P., Bian, H., Carslaw, K. S., Chin, M., Curci, G., Diehl, T., Easter, R. C.,
777 Ghan, S. J., Gong, S. L., Hodzic, A., Hoyle, C. R., Iversen, T., Jathar, S., Jimenez, J. L.,
778 Kaiser, J. W., Kirkevåg, A., Koch, D., Kokkola, H., Lee, Y. H., Lin, G., Liu, X., Luo, G.,
779 Ma, X., Mann, G. W., Mihalopoulos, N., Morcrette, J. J., Müller, J. F., Myhre, G.,
780 Myriokefalitakis, S., Ng, N. L., O'Donnell, D., Penner, J. E., Pozzoli, L., Pringle, K. J.,
781 Russell, L. M., Schulz, M., Sciare, J., Seland, Ø., Shindell, D. T., Sillman, S., Skeie, R.
782 B., Spracklen, D., Stavrou, T., Steenrod, S. D., Takemura, T., Tiitta, P., Tilmes, S.,
783 Tost, H., van Noije, T., van Zyl, P. G., von Salzen, K., Yu, F., Wang, Z., Wang, Z.,
784 Zaveri, R. A., Zhang, H., Zhang, K., Zhang, Q., and Zhang, X.: The AeroCom evaluation
785 and intercomparison of organic aerosol in global models, *Atmos. Chem. Phys.*, 14,
786 10845-10895, 10.5194/acp-14-10845-2014, 2014.

787 Weitkamp, E. A., Sage, A. M., Pierce, J. R., Donahue, N. M., and Robinson, A. L.:
788 Organic aerosol formation from photochemical oxidation of diesel exhaust in a smog
789 chamber, *Environmental Science & Technology*, 41, 6969-6975, 10.1021/es070193r,
790 2007.

791 Ye, P., Ding, X., Hakala, J., Hofbauer, V., Robinson, E. S., and Donahue, N. M.: Vapor
792 wall loss of semi-volatile organic compounds in a Teflon chamber, *Aerosol Science and*
793 *Technology*, 50, 822-834, 10.1080/02786826.2016.1195905, 2016.

794 Yeh, G. K., and Ziemann, P. J.: Alkyl Nitrate Formation from the Reactions of C-8-C-14
795 n-Alkanes with OH Radicals in the Presence of NO_x: Measured Yields with Essential
796 Corrections for Gas-Wall Partitioning, *J. Phys. Chem. A*, 118, 8147-8157,
797 10.1021/jp500631v, 2014.

798 Yeh, G. K., and Ziemann, P. J.: Gas-Wall Partitioning of Oxygenated Organic
799 Compounds: Measurements, Structure-Activity Relationships, and Correlation with Gas

800 Chromatographic Retention Factor, *Aerosol Science and Technology*, 49, 726-737,
801 10.1080/02786826.2015.1068427, 2015.

802 Zhang, X., Pandis, S. N., and Seinfeld, J. H.: Diffusion-Limited Versus Quasi-
803 Equilibrium Aerosol Growth, *Aerosol Science and Technology*, 46, 874-885,
804 10.1080/02786826.2012.679344, 2012.

805 Zhang, X., Cappa, C. D., Jathar, S. H., McVay, R. C., Ensberg, J. J., Kleeman, M. J., and
806 Seinfeld, J. H.: Influence of vapor wall loss in laboratory chambers on yields of
807 secondary organic aerosol, *Proc. Natl. Acad. Sci. U. S. A.*, 111, 5802-5807,
808 10.1073/pnas.1404727111, 2014.

809 Zhang, X., Schwantes, R. H., McVay, R. C., Lignell, H., Coggon, M. M., Flagan, R. C.,
810 and Seinfeld, J. H.: Vapor wall deposition in Teflon chambers, *Atmospheric Chemistry
811 and Physics*, 15, 4197-4214, 10.5194/acp-15-4197-2015, 2015.

812

813

814

815

816

817

818

819

820

821

822

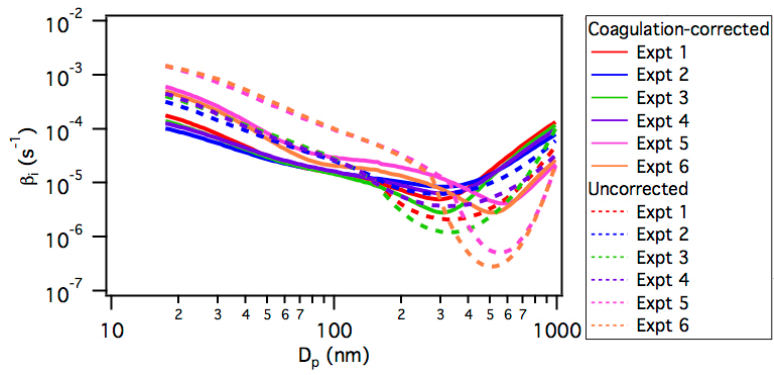
823

824 **Table 1:** Experimental conditions and results

Expt	Experimental Conditions	Initial Seed aerosol Surface area ($\mu\text{m}^2 \text{cm}^{-3}$)	Initial [α -pinene] ^a ($\mu\text{g m}^{-3}$)	ΔM_0 ^{b,c} ($\mu\text{g m}^{-3}$)	SOA Mass Yield ^d (%)
1	0.015 M AS, seed only ^e	1090	-	-	-
2	0.05 M AS, seed only ^e	1190	-	-	-
3	0.015 M & 0.05 M AS, seed only ^e	1470	-	-	-
4	0.015 M & 0.05 M AS, seed only ^e	1210	-	-	-
5	0.05 M AS, seed only ^f	8000	-	-	-
6	0.015 M & 0.05 M AS, seed only ^f	8580	-	-	-
7	0.015 M AS, O ₃ + α -pinene ^{g,i}	1090	281.8±14.9	71.5±0.5	25.4±1.3
8	0.05 M AS, O ₃ + α -pinene ^{g,j}	1260	278.5±13.9	65.9±0.9	23.7±1.2
9	0.05 M AS, O ₃ + α -pinene ^{h,k}	9160	283.8±14.2	74.2±1.9	26.1±1.5
10	0.05 M AS, O ₃ + α -pinene ^{h,k}	8390	265.8±13.3	71.0±3.4	26.7±1.9
11	0.015 M & 0.05 M AS, O ₃ + α -pinene ^{h,l}	8180	289.8±14.5	60.5±1.7	20.9±1.2
12	0.015 M & 0.05 M AS, O ₃ + α -pinene ^{h,l}	9440	271.8±13.6	53.7±2.9	19.7±1.4

825 ^aAll the α -pinene reacted in the 500 ppb O₃ experiments.826 ^bThe SOA mass concentration (ΔM_0) is calculated using the density = 1.37 g cm⁻³
827 obtained from the 500 ppb O₃ nucleation experiment in Nah et al. (2016).828 ^cUncertainties in the peak SOA mass concentration are calculated from one standard
829 deviation of the aerosol volume as measured by the scanning mobility particle sizer.830 ^dSOA mass yields at peak SOA growth are reported.831 ^eReferred to as a “low-SA-seed-only experiment” in the main text.832 ^fReferred to as a “high-SA-seed-only experiment” in the main text.833 ^gReferred to as a “low-SA experiment” in the main text.834 ^hReferred to as a “high-SA experiment” in the main text.835 ⁱSize-dependent particle wall-deposition coefficients obtained from Expt 1 were used for
836 particle wall-deposition correction.837 ^jSize-dependent particle wall-deposition coefficients obtained from Expt 2 were used for
838 particle wall-deposition correction.839 ^kSize-dependent particle wall-deposition coefficients obtained from Expt 5 were used for
840 particle wall-deposition correction.841 ^lSize-dependent particle wall-deposition coefficients obtained from Expt 6 were used for
842 particle wall-deposition correction.

843



844

845 **Figure 1:** Uncorrected (dashed lines) and coagulation-corrected (solid lines) particle
 846 wall-deposition coefficients (β_i) for the low-SA-seed-only (experiments 1 through 4) and
 847 high-SA-seed-only (experiments 5 and 6) experiments. Refer to Table 1 for information
 848 on the AS solution(s) used to generate the seed aerosol and the initial seed aerosol surface
 849 area concentrations in these experiments.

850

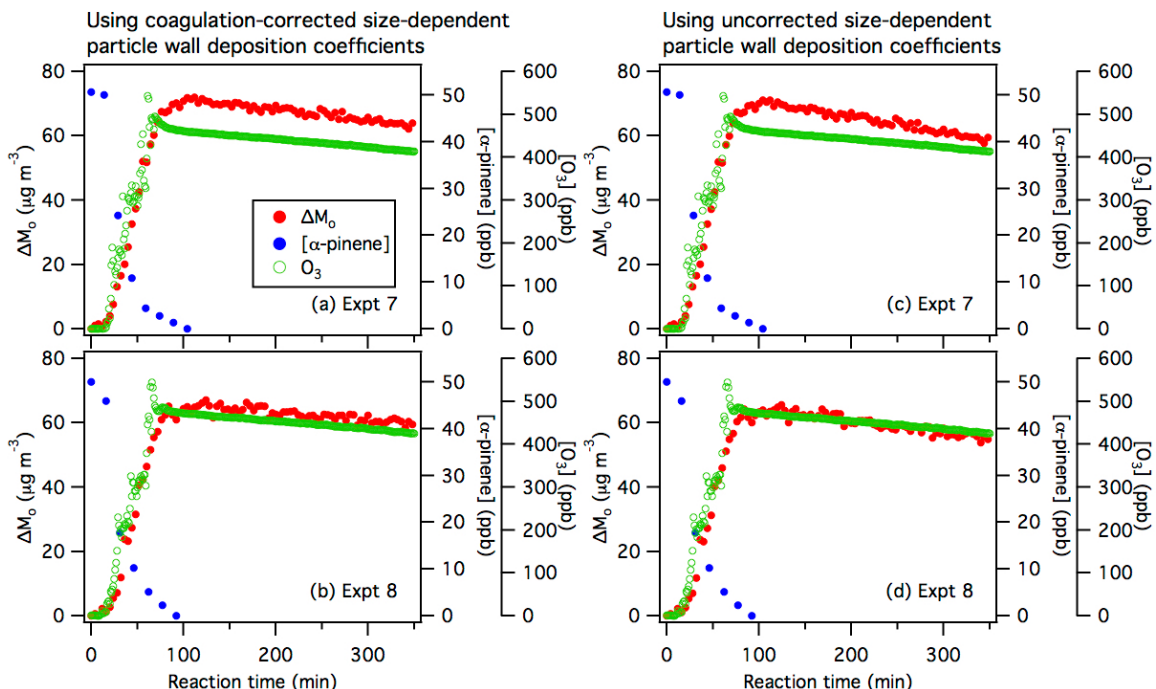
851

852

853

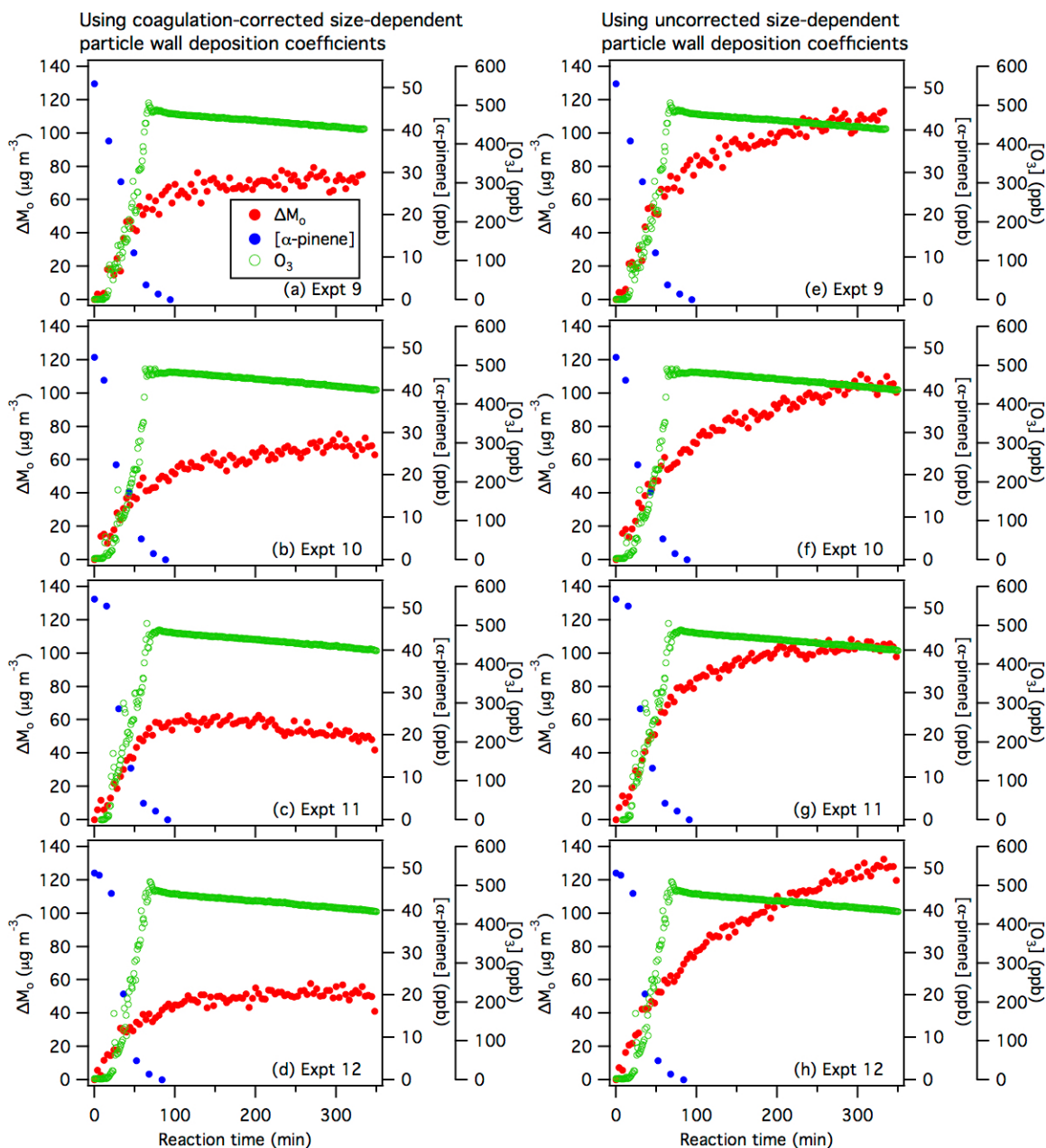
854

855



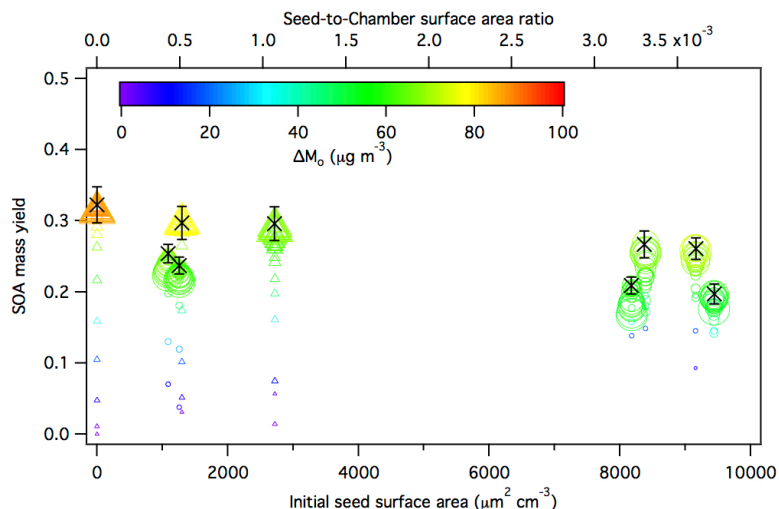
856
857
858
859
860
861
862
863
864

Figure 2: Reaction profiles of the low-SA α -pinene ozonolysis experiments. Panels (a) and (b) show SOA mass concentrations (ΔM_o) obtained using the coagulation-corrected size-dependent particle wall-deposition coefficients from the low-SA-seed-only experiments, while panels (c) and (d) show SOA mass concentrations (ΔM_o) obtained using the uncorrected size-dependent particle wall-deposition coefficients from the low-SA-seed-only experiments. Refer to Table 1 for information on the AS solution(s) used to generate the seed aerosol and the initial seed aerosol surface area concentrations in these experiments.



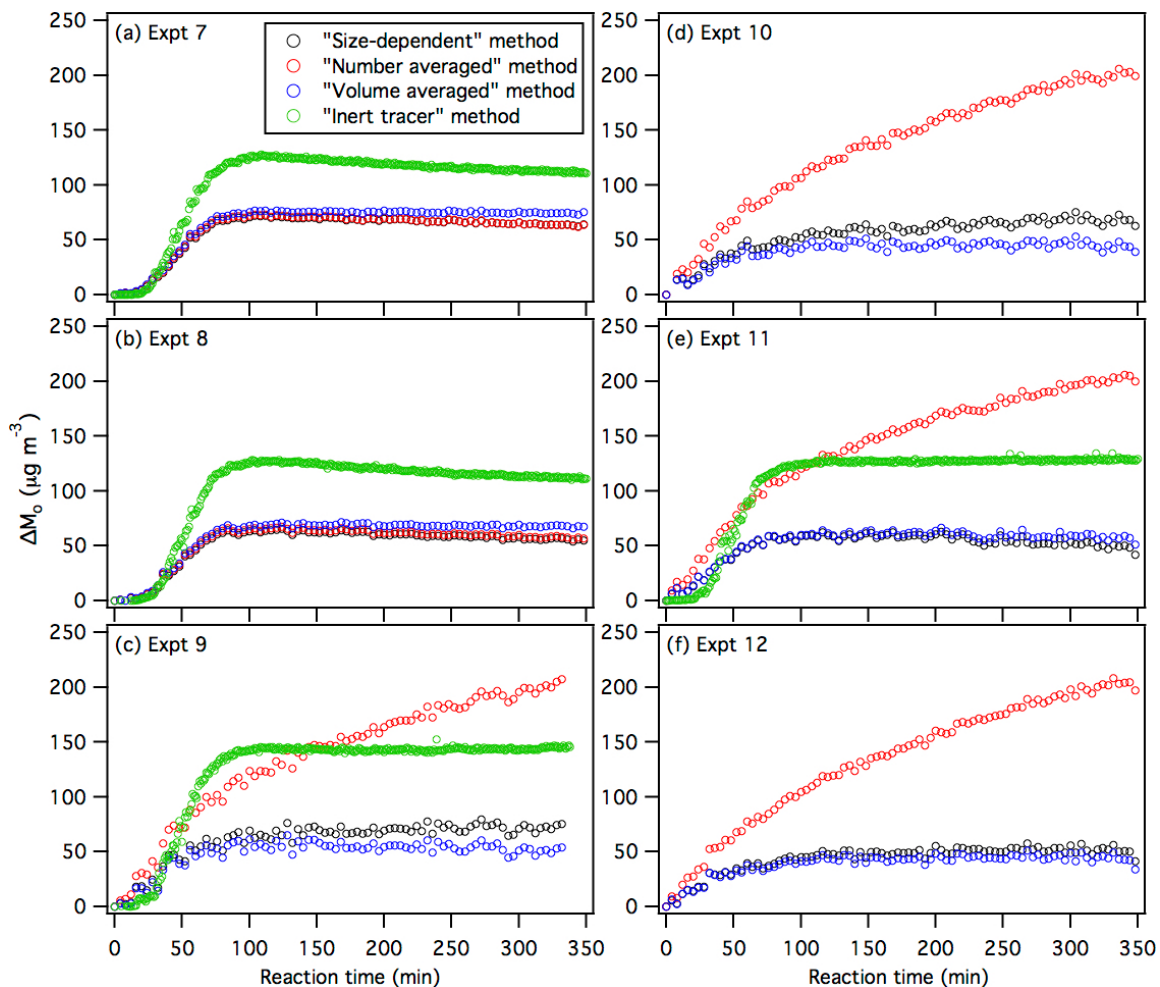
865
866
867
868
869
870
871
872
873
874
875

Figure 3: Reaction profiles of the high-SA α -pinene ozonolysis experiments. Panels (a), (b), (c) and (d) show SOA mass concentrations (ΔM_o) obtained using the coagulation-corrected size-dependent particle wall-deposition coefficients from the high-SA-seed-only experiments, while panels (e), (f), (g) and (h) show SOA mass concentrations (ΔM_o) obtained using the uncorrected size-dependent particle wall-deposition coefficients from the high-SA-seed-only experiments. Refer to Table 1 for information on the AS solution(s) used to generate the seed aerosol and the initial seed aerosol surface area concentrations in these experiments. As explained in the main text, SOA mass concentrations are substantially overestimated when the uncorrected size-dependent particle wall-deposition coefficients are used to account for particle wall deposition.



876

877 **Figure 4:** Averaged SOA mass yields over the course of an α -pinene ozonolysis
 878 experiment as a function of initial total AS seed aerosol surface area concentration.
 879 Results from this study (15 min-averaged) are shown as circles, while results from the
 880 study by Nah et al. (2016) (10 min-averaged) are shown as triangles. All the SOA mass
 881 yields shown here (including results from Nah et al. (2016)) are obtained using the
 882 coagulation-corrected size-dependent particle wall-deposition coefficients. Symbol color
 883 indicates the SOA mass concentration and symbol size indicates the time after O_3 is
 884 injected into the chamber. The \times symbols are the SOA mass yields at peak SOA growth
 885 obtained from the experimental data. The y-axis error bars represent the uncertainty in the
 886 SOA mass yield at peak SOA growth, which originates from the α -pinene injection and
 887 the aerosol mass concentration at peak SOA growth (one standard deviation).



888

889

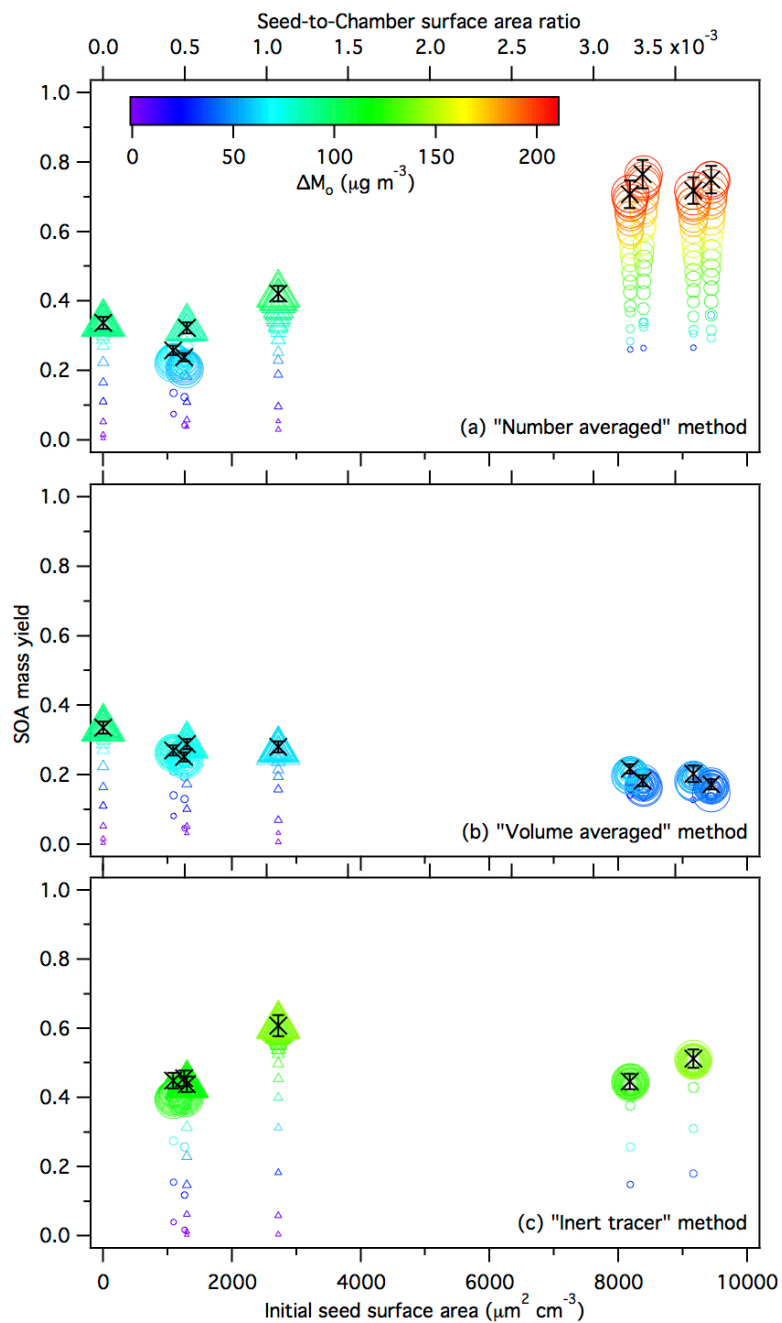
890

891

892

893

Figure 5: SOA mass concentration (ΔM_0) as a function of reaction time in the α -pinene ozonolysis experiments using the “size-dependent”, “number averaged”, “volume averaged” and “inert tracer” particle wall-deposition correction methods. HR-ToF-AMS data were not available in experiments 10 and 12, therefore SOA mass concentrations calculated using the “inert tracer” method were not available in these experiments.



894

895 **Figure 6:** Averaged SOA mass yields over the course of an α -pinene ozonolysis
 896 experiment as a function of initial total AS seed aerosol surface area concentration using
 897 the (a) “number averaged”, (b) “volume averaged” and (c) “inert tracer” particle wall-
 898 deposition correction methods. Results from this study (15 min-averaged) are shown as
 899 circles, while results from the study by Nah et al. (2016) (10 min-averaged) are shown as
 900 triangles. Symbol color indicates the SOA mass concentration and symbol size indicates
 901 the time after O_3 is injected into the chamber. The \times symbols are the SOA mass yields at
 902 peak SOA growth obtained from the experimental data. The y-axis error bars represent
 903 the uncertainty in the SOA mass yield at peak SOA growth, which originates from the α -

904 pinene injection and the aerosol mass concentration at peak SOA growth (one standard
905 deviation).